High confinement modes with radial structure *

D. del-Castillo-Negrete †

B. A. Carreras

V. E. Lynch

Oak Ridge National Laboratory

Oak Ridge TN, 37831-8071

Typeset using REVTEX

*Research sponsored by Oak Ridge National Laboratory, managed by UT-Battelle, LLC, for the U.S. Department of Energy under contract DE-AC05-00OR22725.

†e-mail: delcastillod@ornl.gov

Abstract

We study the radial structure of high confinement modes in a simplified, one-dimensional model of the self-consistent interaction of fluctuations, shear flow, and pressure gradient. The model describes the plasma edge with an energy flux coming from the core, which is used as a boundary condition for the pressure transport equation. As the energy flux increases, there is an L-H transition bifurcation which is described near marginal instability using a reduced Ginzburg-Landau model for the shear flow coupled to a transport equation for the pressure. For higher values of the energy flux, a second transition takes place in which the H mode exhibits a finite-k instability. Numerical results show that this instability leads in the nonlinear regime to the spontaneous formation of a pedestal in the pressure profile, where the effective diffusivity exhibits a sharp drop. A further increase of the energy flux leads to multiple pedestals across the simulation domain.

I. INTRODUCTION

Since the discovery of the L to H transition [1–3], many theoretical models have been proposed, see for example Ref. [4] and references therein. These models involve numerous mechanisms for the creation of transport barriers including ion orbit losses [5,6], Stringer spin-up [7], critical gradients [8], Reynolds stress [9,10], magnetic shear [11,12], and atomic physics [13]. Due to the lack of sufficiently high spatial and temporal resolution, it is difficult to have a clear experimental test to select the dominant mechanisms responsible for the transition. However, recent C-mod experimental results using ECE temperature measurements [14] offer the possibility of improved diagnostics with increased radial resolution during and after the transition. Motivated by this, in this paper we investigate the radial structure of high confinement modes in the context of phase transition models [15–17]

In previous publications [17,18] we discussed the spontaneous formation of shear flows

with nontrivial radial structure in a variant of the flow-fluctuation model presented in Ref. [16]. By spontaneous we mean that, in this model the radial structures arise as nonlinearly saturated finite-k instabilities, and not as a result of externally imposed inhomogeneities. Here we incorporate to the two-fields model a transport equation for the pressure with the corresponding coupling to the fluctuations via a pressure gradient drive. Of particular interest to us is the study of pedestal formation resulting from the plasma self-organization driven by the self-consistent interaction of fluctuations, shear and pressure gradients.

The organization of the rest of the paper is as follows. In Sec. II we introduce the model, explaining the physical meaning of the various terms. Section III presents a study of homogeneous, stationary solutions and their corresponding linear stability properties. In the first part of Sec. IV we use a weakly nonlinear expansion to derive a Ginzburg-Landau model describing the dynamics of the system near marginal instability. The second part of Sec. IV presents numerical solutions of pedestal formation. Section V presents the conclusions.

II. MODEL

Our starting point is the following transport model describing the dynamics of the turbulence fluctuation level $E = \langle (\tilde{n}_k/n_0)^2 \rangle^{1/2}$, the poloidal flow shear, $\langle V_\theta \rangle'$, and the pressure p:

$$\frac{\partial E}{\partial t} = \gamma_0 \left(-\frac{a}{p_0} \frac{\partial p}{\partial x} \right) E - \alpha_1 E^2 - \alpha_2 \langle V_\theta \rangle'^2 E + \frac{\partial}{\partial x} \left[(D_A E + D_0) \frac{\partial E}{\partial x} \right] \tag{1}$$

$$\frac{\partial \langle V_\theta \rangle'}{\partial t} = -\hat{\mu} \langle V_\theta \rangle' + \alpha_3 \langle V_\theta \rangle' E + \frac{\partial^2}{\partial x^2} \left[(D_A E + D_0) \langle V_\theta \rangle' \right] \tag{2}$$

$$\frac{\partial p}{\partial t} = S(x) + \frac{\partial}{\partial x} \left[(D_A E + D_0) \frac{\partial p}{\partial x} \right] . \tag{3}$$

This model is similar to the one originally proposed in Ref. [16], except for the third term on the right hand side of the $\langle V_\theta \rangle'$ equation. As discussed in Ref. [17], this term has been corrected in order to conserve momentum. This is a one-dimensional model in which quantities

are assumed to depend only on the minor radius coordinate, x, with $\langle\ \rangle$ denoting poloidal and toroidal average over magnetic flux surfaces.

The first term in the equation for E represents a pressure driven, linear growth of the fluctuations. Here, a and p_0 are characteristic scales of length and pressure respectively, so that the term in parenthesis is of order one. The second term in the right-hand-side of Eq. (1) models the saturation of turbulence in the L-mode, and the third term models the turbulence suppression by shear flow. The first term in the right hand side of Eq. (2), models the poloidal flow shear damping due to magnetic pumping, and the second term represents the poloidal flow drive by Reynolds stress. Estimates of the parameters α_1, α_2, α_3 and $\hat{\mu}$ are discussed in Ref. [15] for various turbulence models.

The terms involving spatial derivatives, model diffusion. In Eqs. (1) and (3) these terms have the standard Fick's law structure, with D_0 representing the collisional diffusion and $D_A E$ representing a renormalized turbulent diffusion. The apparent different structure of the diffusion operator in Eq. (2) is due to the fact that this is an equation for the shear, the *derivative* of the momentum. The poloidal momentum diffusion itself is modeled using Fick's law, $\partial_x\left[(D_A E + D_0)\partial_x\langle V_\theta\rangle)\right]$ [17].

To reduce the number of independent parameters, we write the model in dimensionless variables as:

$$\frac{\partial \bar{E}}{\partial \tau} = \left|\frac{\partial \bar{p}}{\partial y}\right| \bar{E} - \bar{E}^2 - \sigma^2\,\bar{E} + \frac{\partial}{\partial y}\left[\left(D_1\,\bar{E} + \bar{D}_0\right)\,\frac{\partial \bar{E}}{\partial y}\right] \tag{4}$$

$$\frac{\partial \sigma}{\partial \tau} = -\sigma + a_3\,\sigma\,\bar{E} + \frac{\partial^2}{\partial y^2}\left[\left(D_1\,\bar{E} + \bar{D}_0\right)\,\sigma\right] \tag{5}$$

$$\frac{\partial \bar{p}}{\partial \tau} = \bar{S}(y) + \frac{\partial}{\partial y}\left[\left(D_1\,\bar{E} + \bar{D}_0\right)\,\frac{\partial \bar{p}}{\partial y}\right]\,, \tag{6}$$

where the dimensionless variables are defined as $\tau = \hat{\mu}t$, $y = x/a$, $\bar{p} = p\,\gamma_0/(\hat{\mu}p_0)$,

$$\sigma = \sqrt{\alpha_2/\hat{\mu}}\,\langle V_\theta\rangle'\,, \qquad \bar{E} = (\alpha_1/\hat{\mu})E\,, \qquad \hat{S} = S\,\gamma_0/(p_0\hat{\mu}^2)\,, \tag{7}$$

and we have defined the independent parameters $a_3 = \alpha_3/\alpha_1$, $D_1 = D_A/(a^2\alpha_1)$, $\bar{D}_0 = D_0/(a^2\hat{\mu})$. In these non-dimensional variables, the spatial domain, $y \in (0,1)$, represent the

edge of the plasma. We will assume that the energy source term, $\bar{S}$, is zero in this layer and that the system is driven by an energy flux $\bar{\Gamma}_0$ from the core which determines the boundary condition at $y = 0$ according to

$$\bar{\Gamma}_0 = -\left(D_1\,\bar{E} + \bar{D}_0\right)\,\left.\frac{\partial \bar{p}}{\partial y}\right|_0 . \tag{8}$$

Here we have neglected diamagnetic effects. The role of these effects in the temporal evolution of the L-H transition is considered in Ref. [14]. In the remainder of this paper we present analytical and numerical solutions of the model in Eqs. (4)-(6). First we consider homogeneous solutions representing L and H mode states with no radial structure, and then we present solutions of H-modes with radial structure.

The plasma edge parameters considered here correspond to a low field ($2T$) tokamak with minor radius of $0.5\,m$. We assume that the plasma edge fluctuation level in the L-mode is about $10\,\%$, and that the effective perpendicular diffusion is of order $1\,m^2/sec$. We calculate the poloidal flow-damping rate on the basis of neoclassical theory. For these values, the parameters of the model are $D_1 = 0.01$, $D_0 = 0.001$, and $a_3 = 2$. More detailed comparison with the experiment can be found in Ref. [14] where we also discuss the case of a high field tokamak, the Alcantor C-mod.

III. STATIONARY, HOMOGENEOUS STATES

These solutions, know also as fixed points, are obtained by setting $\partial_\tau = \partial_y = 0$ and solving the resulting algebraic equations. There are three types of fixed points.

Neoclassical fixed point:

$$\bar{E}_0 = 0\,, \qquad \sigma_0 = 0\,, \qquad \left|\frac{\partial \bar{p}}{\partial y}\right|_0 = \frac{\Gamma_0}{\bar{D}_0}\,. \tag{9}$$

We call this solution "neoclassical" because it has no flow or turbulence, and transport is only due to collisional effects. This solution corresponds to a simple, linear pressure profile $\bar{p}_y = \bar{p}(1) = (\bar{\Gamma}_0/\bar{D}_0)(1-y)$.

L-mode fixed point:

$$\bar{E}_L = \left|\frac{\partial \bar{p}}{\partial y}\right|_L , \qquad \sigma_L = 0 , \qquad \left|\frac{\partial \bar{p}}{\partial y}\right|_L = \frac{\sqrt{\bar{D}_0^2 + 4D_1\bar{\Gamma}_0} - \bar{D}_0}{2D_1} . \tag{10}$$

As expected from an L-mode state, this solution has no shear flow, and transport is dominated by turbulence effects with collisional transport playing a minor role. In this state, the confinement time, defined as the integral of the pressure divided by the flux per unit length, is in dimensional units

$$t_L = \frac{a^2}{2}\sqrt{\frac{p_0\alpha_1}{a\gamma_0\Gamma_0 D_A}} . \tag{11}$$

Consistent with the standard deterioration of confinement with power characteristic of the L-mode, t_L decreases with the inverse of the square root of the flux.

H-mode fixed point

$$\bar{E}_H = \frac{1}{a_3} , \qquad \sigma_H = \sqrt{\frac{a_3\,\bar{\Gamma}_0}{a_3\,\bar{D}_0 + D_1} - \frac{1}{a_3}} , \qquad \left|\frac{\partial \bar{p}}{\partial y}\right|_H = \frac{a_3\bar{\Gamma}_0}{a_3\bar{D}_0 + D_1} . \tag{12}$$

This solution corresponds to a high confinement state characterized by the presence of a nonvanishing shear flow, and a turbulence fluctuation level below the L-mode level, i.e. $\bar{E}_H < \bar{E}_L$. It is important to note that the H-mode fixed point exists only when the energy flux exceeds the critical value:

$$\bar{\Gamma}_0 \geq \Gamma_c = \frac{a_3\bar{D}_0 + D_1}{a_3^2} . \tag{13}$$

As expected, the confinement time in this state,

$$t_H = \frac{a^2\alpha_3}{2\hat{\mu}D_A} , \tag{14}$$

is independent of the energy flux.

Having found the homogeneous, stationary states, the next step is to study their linear stability properties. This is important because only stable solutions are physically realizable. Also, the changes in the stability properties of the fixed points as the flux varies, gives rise to bifurcations leading to the L-H transition and to bifurcations leading to states with

nontrivial radial structure. The neoclassical fixed point is unstable whenever $\bar{\Gamma}_0 > 0$, with a growth rate $\lambda = \bar{\Gamma}_0/D_0$. The stability properties of the L and H mode fixed points are less trivial and are summarized in Fig. 1. The L-fixed point is stable in region I but unstable in regions II and III. The vertical line separating regions I and II, $\bar{\Gamma}_0 = \Gamma_c$, gives the instability threshold, and, as discussed before, it also gives the threshold for the appearance of the H-mode which only exist in regions II and III. Thus, when crossing the boundary $\bar{\Gamma}_0 = \Gamma_c$, the L-mode becomes unstable and a bifurcation creates a stable H-fixed point. Since the growth rate is pure real, this is a non-oscillatory instability. The H-fixed point is stable in region II and unstable in region III. The stability boundary dividing these two regions is

$$a_{3c} = \frac{1}{8}\,\frac{(\bar{\Gamma}_0/\Gamma_c - 3)^2}{(\bar{\Gamma}_0/\Gamma_c - 1)}\,. \tag{15}$$

An important property of the H-mode instability in region III, is that it is a *finite-k instability*. That is, the wavenumber of the mode with maximum growth rate,

$$k_m^2 = \frac{(\bar{\Gamma}_0/\Gamma_c - 2)^2 - 1 + 8a_3(\bar{\Gamma}_0/\Gamma_c - 1)}{4D_1(\bar{\Gamma}_0/\Gamma_c - 2)}\,, \tag{16}$$

is nonzero. In Refs. [17,18] we studied the role of these instabilities in the spontaneous formation of shear flows with radial structures in a model involving only the fluctuations $\bar{E}$ and the shear σ. In the following section, we study these type of solutions including the coupling to the pressure transport equation.

IV. HIGH-CONFINEMENT STATES

In this section we study nonhomogeneous high-confinement states. Following the linear stability analysis presented above, we divide the discussion in two parts: H mode solutions for parameter values in region II, and H mode solutions in region III of the stability diagram in Fig. 1.

A. Dynamics near L-H transition point

Consider H-mode solutions near the L-H transition critical point. This corresponds to parameter values in region II, near the stability boundary with region I, e.g. the dashed in Fig. 1. The main advantage of this region is that it is possible to derive a simplified description of the system using a multiple scales perturbation analysis. The first step is to introduce a small parameter δ proportional to the departure from the critical point

$$\bar{\Gamma}_0 = \Gamma_c + \delta^2 \,, \tag{17}$$

where $\delta^2/\Gamma_c \ll 1$. Based on this parameter, we define a slow time variable, $\bar{\tau} = a_3 \delta^2 \, \tau$, and a stretched coordinate $\eta = a_3 \delta \, y/\sqrt{D_1}$, and consider a perturbative expansion of the form

$$\sigma = \delta \, \sigma_1 \qquad \bar{E} = \bar{E}_c + \delta^2 \, \bar{E}_2 \,, \qquad \hat{p} = \hat{p}_c + \delta^2 \, \hat{p}_2 \,, \tag{18}$$

where $\hat{p} = -\partial_y \bar{p}$ is the pressure gradient, and $(\sigma_c, \bar{E}_c, \hat{p}_c)$ is the L-H transition fixed point. Substituting (18) in Eqs. (4)-(6), and equating terms of equal order, we obtain the algebraic relation

$$\bar{E}_2 = \hat{p}_2 - \sigma_1^2 \,, \tag{19}$$

and the dynamical equations

$$\frac{\partial \hat{p}_2}{\partial \hat{\tau}} = \frac{\partial}{\partial \eta^2} \left(2\hat{p}_2 - \sigma_1^2 \right) \,. \tag{20}$$

$$\frac{\partial \sigma_1}{\partial \hat{\tau}} = \sigma_1 \left(\hat{p}_2 - \sigma_1^2 \right) + \frac{\partial^2 \sigma_1}{\partial \eta^2} \,. \tag{21}$$

That is, near the transition point, the turbulence fluctuations $\bar{E}$ are "slaved" to σ and $\hat{p}$, and only two dynamical equations are needed. A transport equation for the pressure gradient, Eq. (20), coupled to and a Ginzburg-Landau equation, Eq. (21), for the shear. The boundary condition for the reduced system,

$$2\hat{p}_2 - \sigma_1^2 \Big|_0 = \frac{a_3}{D_1} \,, \tag{22}$$

follows directly from Eqs. (18) and (8).

The system Eqs. (20)-(21) admits exact analytical solutions. Of particular interest, are time independent, $\partial_{\hat{\tau}} = 0$, constant flux, $2\hat{p}_2(x) - \sigma_1^2(x) = a_3/D_1$, solutions. In this case, Eq. (20) is trivially satisfied, and Eq. (21) reduces to an ordinary differential equation with solution

$$\left|\frac{\partial \bar{p}}{\partial y}\right| = \frac{1}{a_3} + A\left[1 + \tanh^2\left(\frac{y}{W}\right)\right], \qquad \bar{E} = \frac{1}{a_3} + A\,\mathrm{sech}^2\left(\frac{y}{W}\right), \tag{23}$$

where the width W and amplitude A of the profile are given by

$$W = \frac{2D_1}{a_3\sqrt{a_3}\delta}, \qquad A = \frac{\delta^2}{2}\frac{a_3}{D_1}. \tag{24}$$

Figure 2 shows this solution for $a_3 = 0.5$, $D_1 = 0.01$, $\delta^2 = 0.04$, $\Gamma_c = 0.04$, and $\bar{\Gamma}_0 = 0.08$. Compared with the right before-transition solution, p_c (dashed line in Fig. 2), the solution exhibits a steeper gradient. The dotted-dashed line in the figure shows the turbulence fluctuation, $\bar{E}$. As expected from an H-mode state, the effective transport coefficient, $(\bar{D}_0 + D_1\bar{E})$, decreases near the edge.

B. Pedestal formation

As mentioned before, in region III, the H-mode has a finite-k instability. One of the main conclusions of this paper is that, in the nonlinear regime, this instability gives rise to the formation of pedestals in the pressure profile. To explore these solutions we integrated numerically Eqs. (4)-(6) with the boundary condition (8). Guided by the linear stability analysis, we fixed $a_3 = 2$, $D_1 = 0.01$, $\bar{D}_0 = 0.001$ and made a scan of the energy flux, $\bar{\Gamma}_0$, from values in region II before the transition, to values deep inside region III where the H mode is unstable. Following a transient, the numerical solutions settle into time independent solutions with radial structure.

For energy fluxes in region II the solutions exhibit the steeper gradient characteristic of the H-mode, qualitatively similar to the one observed with the near-transition Ginzburg-Landau model in Eqs. (20)-(21). The dynamics in region III is more interesting. There, as

shown in Figs. 3 and 4, the numerical results exhibit the spontaneous formation of pedestals in the pressure profile, accompanied by sharp depletions in the turbulence. In Fig. 3, the energy flux, $\bar{\Gamma}_0 = 0.4$, is close to the finite-k instability boundary and a pedestal clearly forms around 0.8. Figure 4 shows the formation of a "double" pedestal for $\bar{\Gamma}_0 = 1.6$. The appearance of multiple pedestal as the energy flux increases, is consistent with the linear stability analysis according to which the wavenumber of the most unstable mode, Eq. (16), increases with $\bar{\Gamma}_0$.

There is an issue on the accessibility of states with multiple pedestals. The power required to access them is higher than for a single pedestal. Because the increase of the power input in the edge plasma region is not instantaneous, but the flux from the core increase continuously, the edge transition will happen at the lowest power accessible state. A more detailed transport model is required to study the evolution of the plasma when the power continuously increases and the plasma is in the H-mode state.

V. CONCLUSIONS

Motivated by the experimental possibility of high spatial resolution diagnostics, we investigated the radial structure of high confinement modes in a simplified model describing the self-consistent interaction of fluctuations, shear flow, and pressure gradient. The model describes the plasma edge with an energy flux, $\bar{\Gamma}_0$, coming from the core, which is used as a boundary condition for the pressure transport equation. It is observed that when the energy flux reaches a threshold, $\bar{\Gamma}_0 = \Gamma_c$, there is a bifurcation in which the L-mode becomes unstable and a stable H-mode appears. Using a multiple scales, weakly nonlinear expansion, we derived a Ginzburg-Landau model describing the dynamics near marginal stability. Analytical solutions of the reduced model show a reduction of effective transport coefficient $\chi_{eff} = D_1 \bar{E} + \bar{D}_0$ near the plasma edge, characteristic of the L-H transition. More interesting is the new finding that for higher values of the energy flux, a second transition takes place in which the H mode exhibits a finite-k instability. Numerical results show that this

instability leads in the nonlinear regime to the spontaneous formation of a pedestal in the pressure profile where $\chi_{eff} = D_1 \bar{E} + \bar{D}_0$ exhibits a sharp drop. As the the energy flux increases, multiple pedestals can be observed, consistent with the fact that the wavenumber of the most unstable mode increases with $\bar{\Gamma}_0$. What is particularly interesting of this model is that the radial structure emerges spontaneously as a result of a finite-k, "pattern forming" instability, and not because of an externally imposed inhomogeneity. We have neglected diamagnetic effects. The role of these effects in the temporal evolution of the L-H transition is discussed in Ref. [14].

Acknowledgments

The thanks A. E. Hubbard for interesting conversations on the experimental aspects of the L-H transition. This work was sponsored by the Oak Ridge National Laboratory, managed by UT-Battelle, LLC, for the U.S. Department of Energy under contract DE-AC05-00OR22725.

REFERENCES

[1] Wagner, F. , *et al.* 1982 *Phys. Rev. Letters* **49**, 1408.

[2] Burrell, K.H., *et al.* 1989 *Plasma Phys. Control. Fusion* **29**, 1959.

[3] Groebner, R.J., *et al.* 1993 *Phys. Fluids B* **5**, 2343.

[4] B. A. Carreras 1997 *IEEE Trans. Plasma Sci.* **25**, 1281.

[5] K. C. Shaing and E. C. Grume 1989 *Phys. Rev. Lett.* **63**, 2369.

[6] S.-I. Itoh and K. Itoh 1988 *Phys. Rev. Lett.* **60**, 2276.

[7] A.B. Hassam, T.M. Antonsen, J. Drake and S.C. Liu 1991 *Phys. Rev. Lett.* **66**, 309.

[8] F. L. Hinton and G.M. Staebler 1993 *Phys. Fluids B* **5**, 1281.

[9] P. H. Diamond, and Y. B. Kim 1991 *Phys. Fluids B* **3** ,1626.

[10] B. A. Carreras, V. E. Lynch and L. Garca 1991 *Phys. Fluids B* **3**,1438.

[11] C. Kessel *et al.* 1994 *Phys. Rev. Lett.* **72**, 1212.

[12] E. Synakowski 1994 *Phys. Plasmas* **4**, 1736.

[13] K.C.Shaing 1992 *Phys. Fluids B* **4**, 171.

[14] A. E. Hubbard , *et al.* 2003 submitted to *Plasma Phys. Control. Fusion* (this volume).

[15] P. H. Diamond, Y-M. Liang, B. A. Carreras, and P. W. Terry 1994 *Phys. Rev. Lett.* **72**, 2565.

[16] P. H. Diamond, V. B. Lebedev, D. E. Newman, and B. A. Carreras 1995 *Phys. Plasmas*, **2**, 3685.

[17] D. del-Castillo-Negrete and B. A. Carreras 2002 *Phys. Plasmas*, **9**, 118.

[18] D. del-Castillo-Negrete, B. A. Carreras, and V. Lynch 2002 *Physica D*, **168-169**, 45-60.

FIGURES

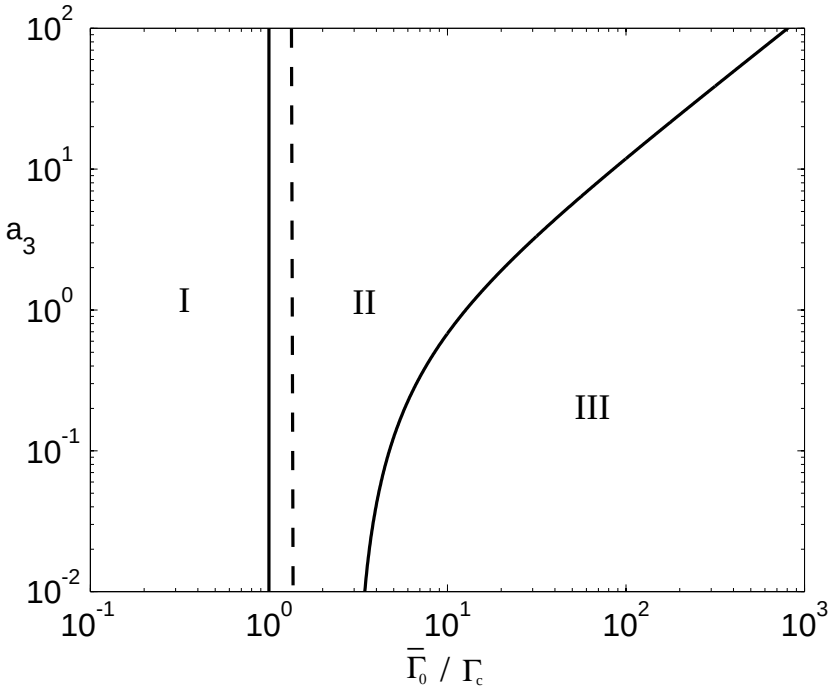

FIG. 1. Stability diagram of the low confinement (L) and high confinement (H) homogeneous, stationary (fixed point) solutions as function of a_3 and the energy input flux $\bar{\Gamma}_0/\Gamma_c$, in the model in Eqs. (4)-(6). The L fixed point is stable in region I and unstable elsewhere. The H fixed point only exists in regions II and III. Crossing the solid vertical line, $\bar{\Gamma}_0 = \Gamma_c$, gives rise to the L-H transition during which the L mode becomes unstable and a stable H mode appears through a pitchfork bifurcation. The H mode is stable in region II, but it is unstable to finite-k instabilities in region III that give rise in the nonlinear regime to pedestal formation (see Figs. 3 and 4. The dashed line marks the region of weak instability described by the Ginzburg-Landau reduced model in Eqs. (20)-(21).

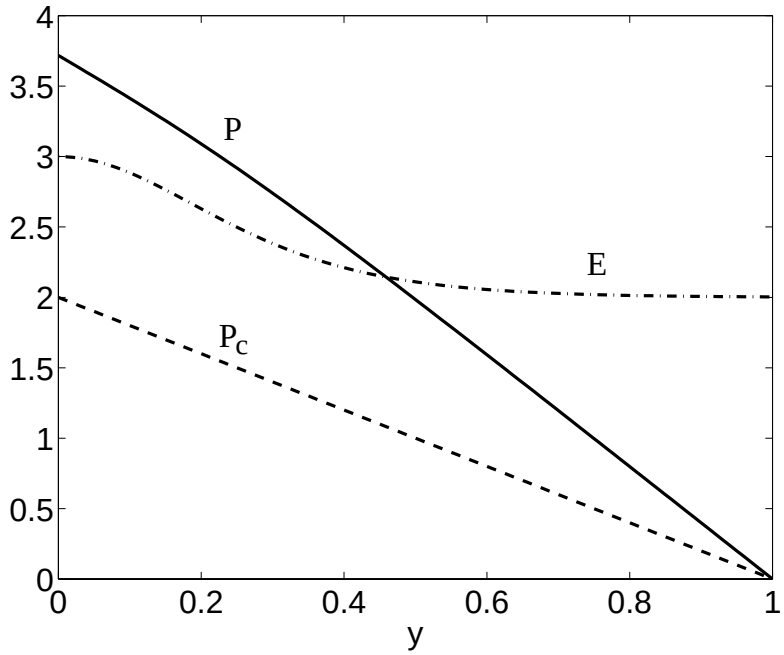

FIG. 2. Solutions of the Ginzburg-Landau reduced model of Eqs. (20)-(21) describing the dynamics near the critical transition point (dashed line in Fig. 1). The dashed line, P_c, is the homogeneous (constant pressure gradient) solution at the critical point. The solid line, P, is the high confinement pressure profile according to solution (23). The dotted-dashed line denotes the turbulence fluctuations E which, as expected, decrease at the edge

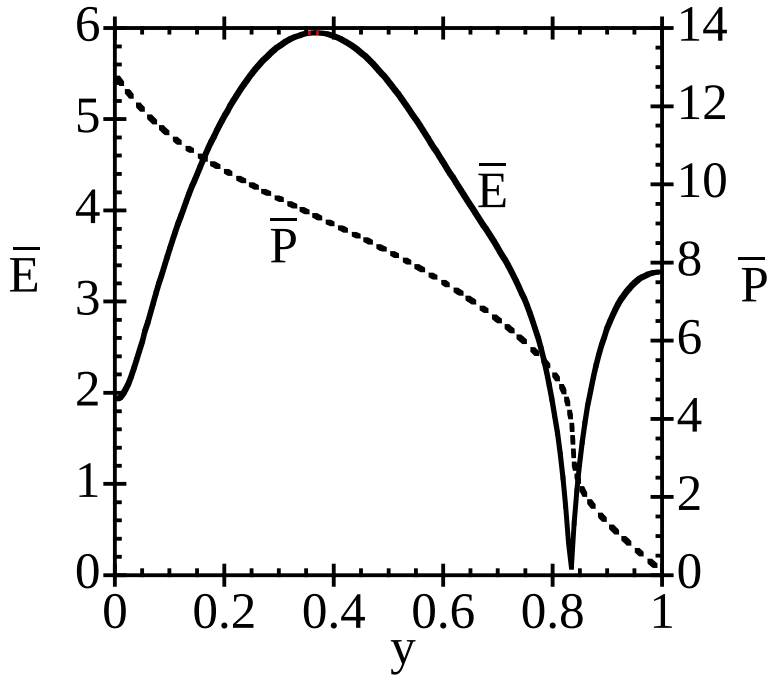

FIG. 3. Self-consistent, spontaneous pedestal formation in the L-H transition obtained from the numerical integration of Eqs. (4)-(6) with $a_3 = 0.5$ and $\bar{\Gamma}_0/\Gamma_c = 9.52$. The pedestal formed in the pressure profile $\bar{P}$ is accompanied by a sharp drop in the turbulence that gives rise to a sudden reduction of the effective transport coefficient, $\chi_{eff} = D_1\bar{E} + \bar{D}_0$, at the edge.

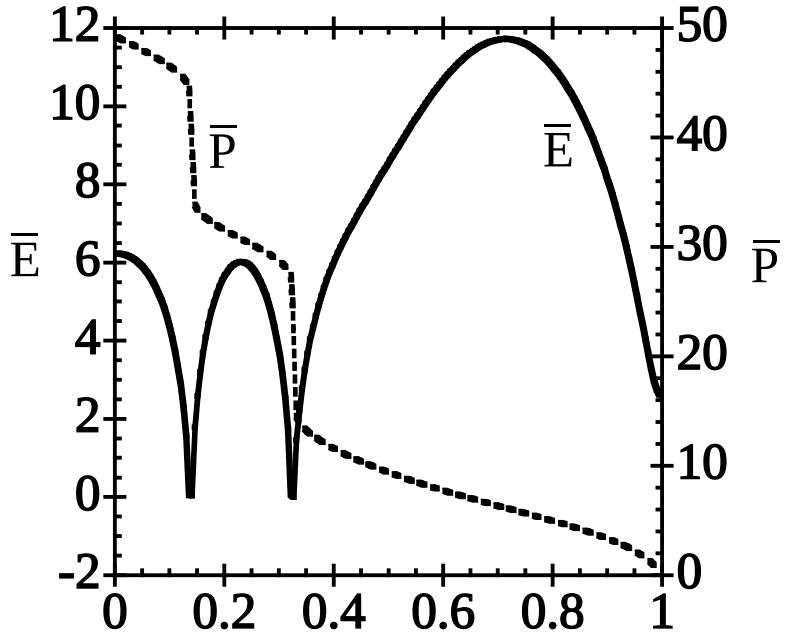

FIG. 4. Same as Fig. 3 except that $\bar{\Gamma}_0/\Gamma_c = 38.09$. For this higher value of the energy flux, the linear stability analysis predicts (see Eq. (16)) a higher wavenumber instability that explains the formation of a double pedestal.